JOURNAL OF MATERIALS SCIENCE 28 (1993) 942–948

Microstructural observation of Nb_3Al multifilamentary superconducting wires

AKIRA HASEGAWA, TAKAO TAKEUCHI, KIYOSHI INOUE
National Research Institute for Metals, Tsukuba Laboratories, 1-2-1 Sengen, Tsukuba-shi, Ibaraki 305, Japan

A sample preparation technique is developed for the transversal observation of Nb tube processed multifilamentary wire. Microstructure characterization of the cross-section of Nb–25 at % (Al–2 at % Cu) wire has been carried out with analytical transmission electron microscopy. Intermetallic compound phases of A15, σ and $NbAl_3$ are observed in a specimen heat-treated at 1023 K. Volume fraction changes of the individual phases indicate that σ and $NbAl_3$ phases formed at the prior Al-core region in the early stage of the heat treatment, and thereafter A15 phase particles grew and coalesced with each other, consuming Nb and σ phase. A change in the volume fraction of A15 phase is correlated with superconducting properties.

1. Introduction

The A15-type phase superconductor Nb_3Al has been considered as a promising superconducting magnet material for high-magnetic-field application such as a fusion reactor magnet [1]. Various fabrication techniques, such as niobium tube [2], jelly roll [1, 3], powder metallurgy (p/m) [4] and clad tip extrusion [5] processes, have been developed to produce superconducting composite wires of practically useful length. These processes are characterized by the reactions between thin Nb and Al layers at relatively low temperatures (< 1300 K) and are thereby of great advantage for obtaining a continuous multifilamentary structure.

Nb_3Al multifilamentary wire prepared by the Nb tube process (filament number: 1.8 million, filament diameter: about 100 nm) shows excellent properties of high critical current density (J_c) [5], upper critical field (H_{c2}) [6, 7], high strain tolerance and low a.c. loss [8]. Adjustment of the hardness of Al cores relative to the Nb matrix by alloying Al cores with additives like Mg, Ag, Cu, Zn, etc. remarkably improves the cold workability of Nb–Al composites [5, 9, 10]. Details of the Nb tube process were presented elsewhere [5]. The superconducting properties of the wire have strong correlations with the microstructure, which is affected by the size of the final filament and the addition of third elements.

Transmission electron microscopy (TEM) studies on these multifilamentary wires can provide direct microstructural information which cannot be obtained from X-ray diffraction (XRD) techniques. This microstructural information about the reaction at the Nb–Al interface will be useful in determining optimum conditions for Nb–Al superconducting wire processing. It is, however, difficult to prepare thin foil specimens for TEM observation since the multifilamentary wire has an inhomogeneous structure. Recently, several studies have been reported concerning cross-sectional observation in multilayered Nb–Al [11, 12], P/M processed wires [13, 14] and a multifilamentary wire [15]. We reported microstructural observations on a transversal cross-section of Nb–(Al–2Cu) multifilamentary wire [7] which had a filament diameter of 320 nm. Compared with longitudinal observation [14], transversal observation is useful for studying the microstructure in a bundle of ultrafine filaments because the configuration of the filaments can be observed directly. The effect of the morphology of Nb–Al composites on phase formation and the interaction between Al cores can also be studied by transversal observation.

In the present study, the effects of reaction time and Al core size on the formation process of A15 have been investigated by transversal observation, and then some possibilities are suggested for improving the superconducting properties of the multifilamentary wire.

2. Experimental procedure

The starting composite material consisted of an Nb tube of 7 and 14 mm inner and outer diameter, respectively, and an inserted Al– 2 at % Cu alloy rod of 6.9 mm diameter. The average composition was about Nb–25 at % (Al– 2 at % Cu). This single-core composite was cold drawn to a wire of 1.14 mm diameter. A bundle of 121 drawn composite wires was inserted into a Nb tube (1st-level stack) and then drawn again. The bundling and drawing processes were repeated twice more (2nd- and 3rd-level stack), and then multifilamentary wires containing 1.8 million ($121 \times 121 \times 121$) ultrafine filaments were fabricated. Microstructural studies were performed on two kinds

0022–2461

of multifilamentary wire with different Al core sizes. One was designated as "sample 1", whose final Al core diameter was 320 nm, and the other as "sample 2", which had a smaller Al core diameter 90 nm and the optimum superconducting properties of Nb–(Al–2Cu) wire [5]. The values of Al core diameter were calculated from the degree of wire drawing. The diameter of each multifilamentary wire was adjusted to be about 3 mm for TEM specimen preparation. The final composite wires were heat-treated at 1023 K for 10.8 ks (3 h) or 86.4 ks (24 h). Detailed features of these samples are given in Table. I.

Fig. 1 shows optical micrographs of lightly electrochemically etched specimens which were heat-treated for 86.4 ks. The cell shown in Fig. 1a corresponds to a 2nd-level stack (121 × 121 bundle) in sample 1. The arrow in Fig. 1a indicates a 1st-level stack of wires which contains 121 single-core composites.

TABLE I Al core size of samples and heat-treatment conditions

Sample	Al core diameter		Heat treatment time at 1023 K (ks)
	Desired[a]	Achieved[b] (d_c)	
1	320 nm	310 nm	10.8 or 86.4
2	90 nm	120 nm	10.8 or 86.4

[a] Calculated from wire drawing ratio.
[b] Estimated from mean separation of Al cores by TEM.

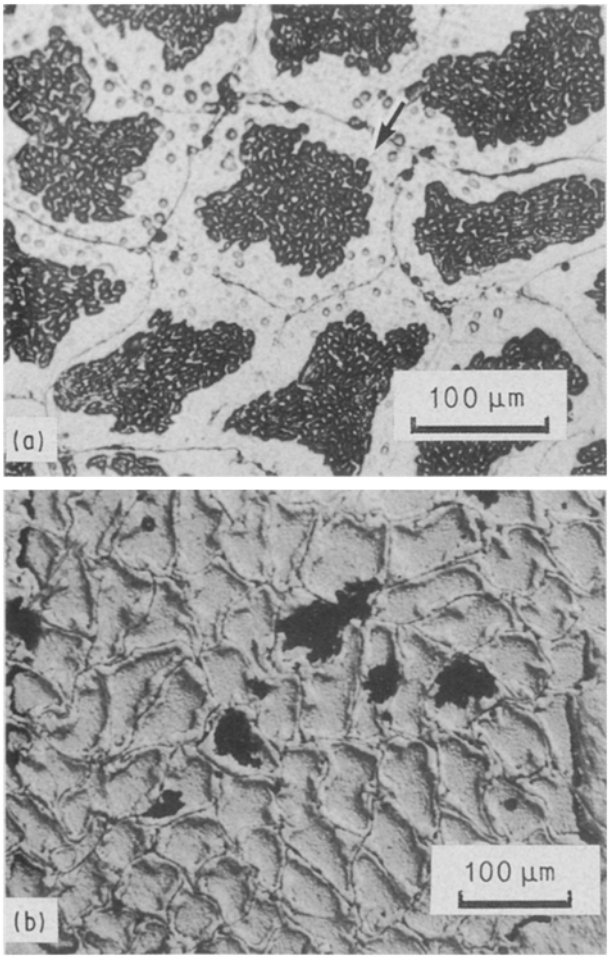

Figure 1 Optical micrographs of Nb–Al multifilamentary wires after heat treatment at 1023 K for 86.4 ks. (a) Sample 1; The arrow indicates the 1st-level stack of Nb/Al composites. (b) Sample 2.

A thin foil specimen for TEM observation was prepared as follows:

(i) Discs of 3 mm diameter were sliced from a transversal cross-section of the wire.

(ii) The disc surfaces were mechanically polished with emery paper.

(iii) One of the surfaces was ground with a dimple grinding machine down to a final specimen thickness of about 50 μm.

(iv) Two-step electropolishing was carried out with a single-jet machine. The flat side was polished lightly and then the dimple-ground side was polished until perforation occurred. The electropolishing was carried out at 243 K with the polishing chemical a mixture of 10% perchloric acid and 90% methanol. These polishing conditions were not suitable for the Nb phase and a chemically passive film was formed on the surface during the process. It was necessary to remove the reaction products frequently until perforation occurred. The electropolishing is an important process to obtain a thin-foil specimen which has a wide observation area.

(v) Argon ion-milling was given to the perforated specimen, using a sample stage cooled by liquid nitrogen.

TEM observation and energy-dispersion X-ray (EDX) analysis were carried out using an analytical electron microscope (JEOL 2010) at 200 kV. The nominal beam diameter for microanalysis was approximately 20 nm, while the effective diameter of the detectable area was estimated to be about 50 nm from the contamination spot size on the specimen. A standardless analytical method was used to obtain Nb/Al composition ratios in the reaction phase. An estimation of Cu in the Al–2Cu core could not be made since background noise of X-rays from the TEM chamber was comparable to the signal from the Al–Cu core. Selected-area diffraction (SAD) and dark-field microscopy were also employed to characterize the phases of solid-state reactions.

3. Results and discussion

3.1. Microstructure of as-drawn specimens

Fig. 2 shows TEM micrographs of as-drawn wires at low magnification. The observation area of Fig. 2a (sample 1) corresponds to the spot indicated by an arrow in Fig. 1a. Since the thin foil specimen has a wide observation area as shown in Fig. 2b (sample 2), it is possible to observe the whole microstructure of a 1st-level stack of wires. The bright image region in the figures corresponds to the Al core. The average Al core size (d_c) of the specimen was estimated from the mean distance between the Al cores (L_c), assuming $L_c = 2d_c$ for the original Nb–Al composite configuration. The estimated values are approximately 310 nm in sample 1 and 120 nm in sample 2. The estimated Al core size of sample 2 was, however, larger than that

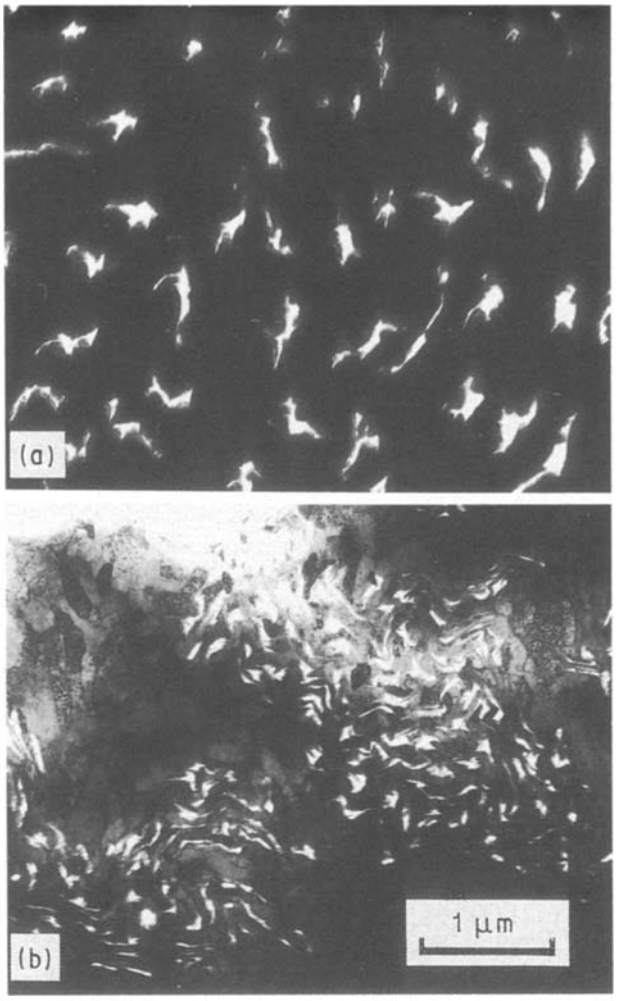

Figure 2 TEM micrographs of the cross-section of as-drawn specimens in a low-magnification condition: (a) sample 1, (b) sample 2.

calculated from its drawing ratio. This was due to irregular deformation of the filament, i.e. the so-called "sausaging" effect.

Fig. 3 shows TEM micrographs of the as-drawn specimens. The ribbon-like morphology of the Al core is clearly seen in this figure. The typical appearance was reported in P/M-processed wires [4]. In Fig. 3b an ultrathin multilayered structure is found within the Al core. The cross-section has two characteristic regions, labelled A and E. Dark region A was identified by EDX as an Nb matrix, and E was an Al core. Interfaces of the regions A and E were easily distinguished because the microstructures of these phases were quite different from each other. Region A contains considerable dislocations that show the cold-worked structure produced by drawing. On the other hand, twins, dislocations and grain boundaries were not found in region E. Determination of the crystal structure of region E by SAD was not successful, because of its amorphous-like diffraction pattern. Highly disordered Al produced by the fabrication process was reported in P/M-processed wire [16].

The Nb/Al atomic ratio in region E varied from 85/13 to 32/68. The high Nb concentration in region E (Al core) may be attributed to the multilayered structure (Nb/Al/Nb/Al/ . . .) which was shown in Fig. 3b, and the Nb/Al ratio in the multilayered structure may

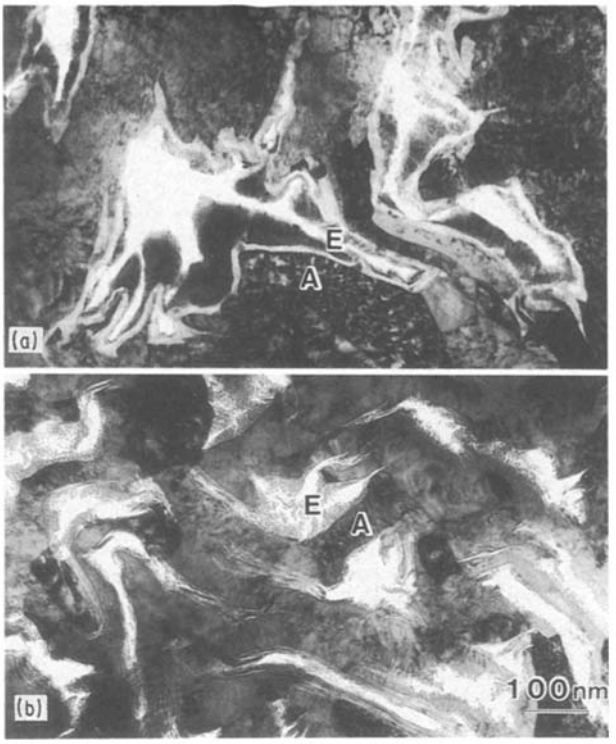

Figure 3 Enlarged TEM micrographs of the cross-section of as-drawn specimens: (a) sample 1, (b) sample 2.

be magnified by preferential sputtering of Al during the ion-milling process. A kind of mechanical alloying in the Al core region was strongly suggested by the EDX analysis, taking account of the ribbon-like morphology and the multilayered structure.

3.2. Microstructure of heat-treated specimens

Fig. 4 shows TEM micrographs of sample 1 which

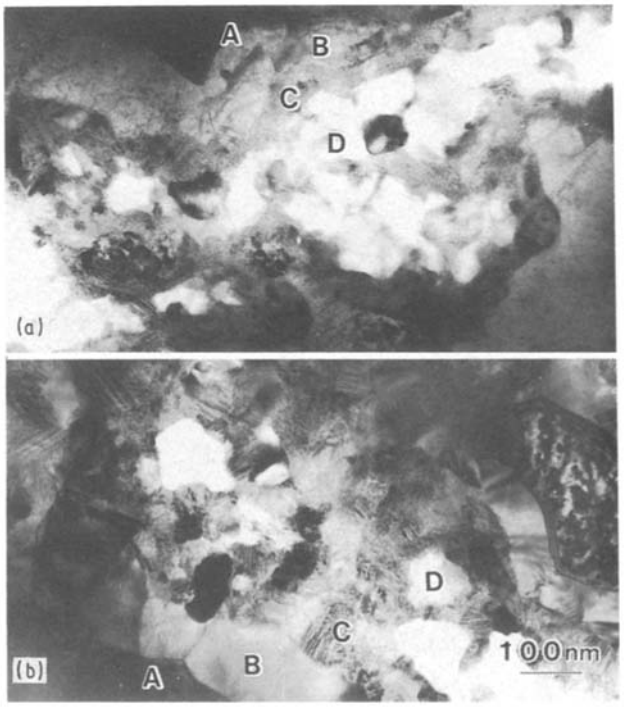

Figure 4 TEM micrographs of the cross-section of sample 1: heat-treated at 1023 K for (a) 10.8 ks (b) 86.4 ks.

TABLE II Chemical composition ratio of Nb/Al (at%) in each region

Specimen	Region	Nb/Al		
		As-drawn	1023 K × 10.8 ks	1023 K × 86.4 ks
Sample 1	A	97–100/0–3	85–100/0–15	94–100/0–6
	B	–	[a]	77–86/14–23
	C	–	62–68/32–38	60–72/28–40
	D	–	32–38/62–68	42–43/57–58
	E	32–85/15–68	–	–
Sample 2	A	97–100/0–3	91–100/0–9	96–98/2–4
	B	–	75–81/19–25	76–82/18–24
	C	–	62–69/31–38	66–72/28–34
	D	–	33–42/58–67	[a]
	E	50–88/12–50	–	–

[a] The size of the phase was smaller than the spatial resolution of EDX.

was heat-treated for 10.8 or 86.4 ks. Microstructures were divided into four regions A, B, C and D. Compositions of each phase are summarized in Table II. In Fig. 4a, region D, which has a bright image, consisted of several grains of 50 to 100 nm in size. The details of the phase will be shown later. Region C showed opaque grain boundary contrast and fine twin images. The region is identified as σ (Nb_2Al) phase, as judged from its Nb/Al composition ratio (Nb/Al: 62–68/32–38). Region A (Nb) does not show any significant differences in microstructure, compared with an as-drawn specimen. Other phases with small grains were frequently found in the area between regions A and C, which was classified as region B. The microstructure of region B was simple, without dislocations and twins. The grain length of B was approximately 100 nm and the grain width was less than 50 nm. Since the grain size was almost the same as the spatial resolution of microanalysis, the Nb/Al atomic ratio of region B changes gradually.

Fig. 4b shows the microstructure of the wire after 86.4 ks treatment. Compared with Fig. 4a, region D had shrunk and the finer twin images of C became dominant. The image of the fine twins was a characteristic feature inherent in the σ phase [9, 13]. The grain growth of B was considerable. It is noted that a single layer of A15 grains formed at the border of region C. The grain length of B along the border of C was about 200 nm and its layer thickness (grain width) was about 100 nm. The SAD analysis showed that B was of A15 type (Nb_3Al). The composition ratio of region B almost coincided with the A15 phase composition. The microstructure of the remaining Nb did not show any significant differences, as compared with an as-drawn specimen. A small amount of Al (4–6 at %) in the remaining Nb was detected in the vicinity of the A–B interface.

Voids were observed in region D of the specimen reacted for 10.8 ks. Fig. 5a is an enlargement of region D and voids are indicated by arrows. The micrograph was taken in an under-focus condition. The voids in region D were not found in the specimen reacted for

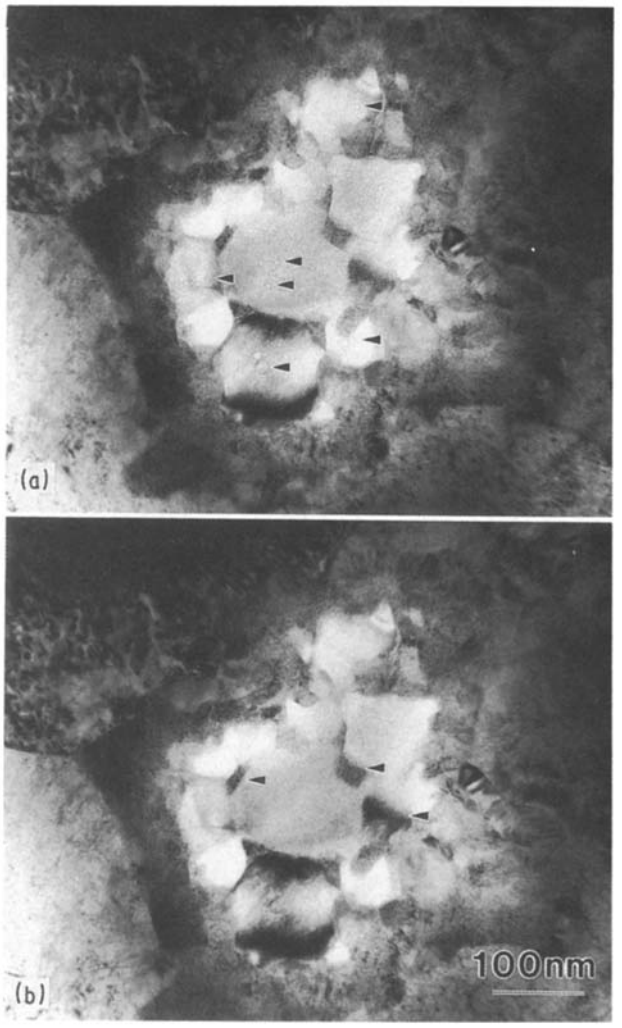

Figure 5 Enlarged TEM micrographs of a central part of the reaction phase in sample 1 (heated at 1023 K for 10.8 ks). (a) Under-focus condition; the arrows indicate voids. (b) Just-focus condition; the arrows indicate σ phase in the grain boundary of $NbAl_3$.

86.4 ks. The void formation may result from the Kirkendall effect of Al diffusion into Nb in the early stage of the phase formation sequence. The fast Al diffusion compared to Nb may be ascribed to the large areal reduction ratio of the wire which increased the mobility of atoms [17]. SAD analysis showed that the grain containing voids was $NbAl_3$. Fig. 5b, taken in a just-focus condition, shows the presence of σ phase between grain boundaries of $NbAl_3$. A deviation from stoichiometric σ or $NbAl_3$ phase composition in region D may be attributed to the dual phase structure.

Fig. 6 shows micrographs of sample 2. Microstructures of each phase had basically the same features as in sample 1. In Fig. 6a the grain size of $NbAl_3$ was smaller than that of sample 1. Voids were also observed in the $NbAl_3$ grains. Region C gave an opaque image. The grain size of A15 was almost the same as that of sample 1 but the A15 phase occupied a larger part of the cross-section. Fig. 6b shows the microstructure of the wire after 86.4 ks treatment. Region D occupied a smaller part of the area than in Fig. 4b. Since the area of region D was smaller than the spatial resolution of EDX analysis, no difference of Nb/Al ratio between D and C was detected. No voids were

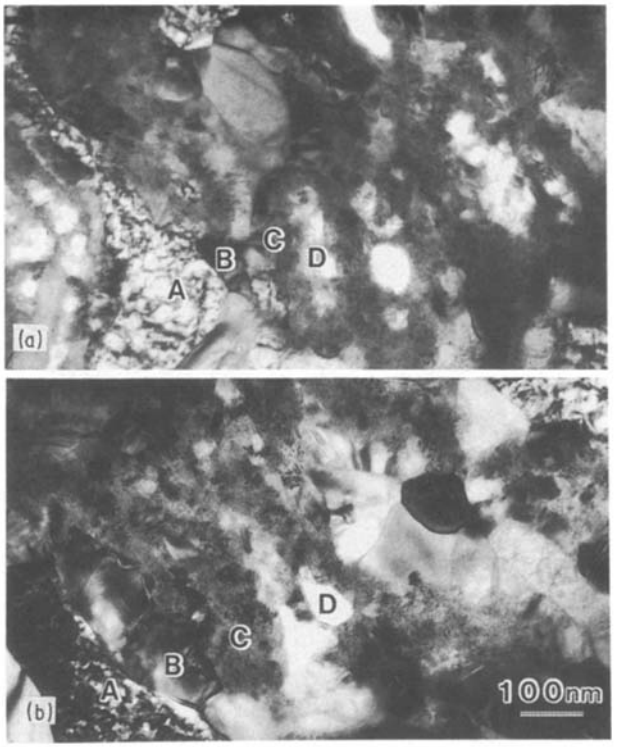

Figure 6 TEM micrographs of cross-sections of sample 2: heat-treated at 1023 K for (a) 10.8 ks, (b) 86.4 ks.

TABLE III The result of phase characterization

Region	A	B	C	D	E
Phase	Nb	A15 (Nb_3Al)	σ (Nb_2Al)	$\sigma + NbAl_3$	Al core

observed in region D. Region C also had an opaque image. Clear, fine twin images as in sample 1 were not observed. The A15 grains were equiaxed and the grains coupled with each other to form a large aggregation of A15. Coarse twins were frequently found in the A15 grains. The composition ratio of Nb/Al ranged over 76–81/19–24. A small amount of Nb remained in the A15 aggregate.

The results of the phase characterization are summarized in Table III. The Nb/Al composition ranges of these reaction phases were wider than those predicted by the equilibrium phase diagram, presumably due to the non-equilibrium nature of the reaction process.

3.3. Reaction phase distribution

Fig. 7 shows schematic phase distributions of sample 1 after heat treatment, based on the above classification. The hexagons in the figure indicate the initial Nb/Al composite size assuming close packing in the 1st-level stack. Since the cold working was not uniform in the transversal cross-section, the Al core separation was not constant. When the distance between Al cores was short, σ phase formation occurred rather than A15 formation because of insufficient Nb in the early stage of the phase formation sequence. The

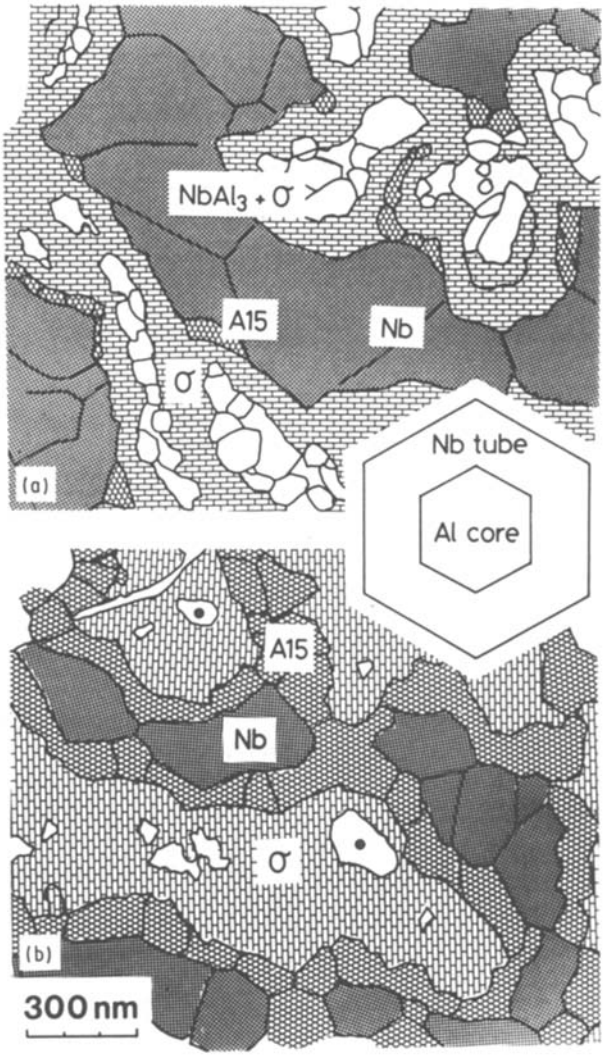

Figure 7 Schematic representation of cross-sectional microstructure of sample 1 based on the phase classification: heat-treated at 1023 K for (a) 10.8 ks, (b) 86.4 ks. The hexagons indicate the initial Nb–Al composite size assuming closed packing in the 1st-level stack; (●) indicates perforation.

Nb, A15, σ and $NbAl_3$ phases coexisted when the Al core separation was large. In Fig. 7b, a sheath configuration of A15 and its coupling were seen. A15 phase interconnection in the 1st-level stack was also found in sample 2, as is shown in Fig. 8. The sheath shape of A15 in sample 2 was not obvious because it formed a larger aggregate of A15 than that of sample 1. A large part of the σ phase remained and a small amount of unreacted Nb was found in the 1st-level stack of sample 2.

Area fractions, i.e. volume fractions, of each phase in the 1st-level stack are summarized in Fig. 9. These values are the average of five measurements for different observed areas of which the size was about 1.2 μm × 1.8 μm wide. The number of filaments in the each observed area was 5 to 8 in sample 1 and 40 to 50 in sample 2.

In sample 1 for 10.8 ks treatment, the volume fraction of region C (σ) plus D ($\sigma + NbAl_3$) is almost the same as that of Al cores of the as-drawn specimen and the volume fraction of A15 is small. This implies that the σ and $NbAl_3$ phases formed in prior Al core regions and A15 precipitated from the Nb–σ interface.

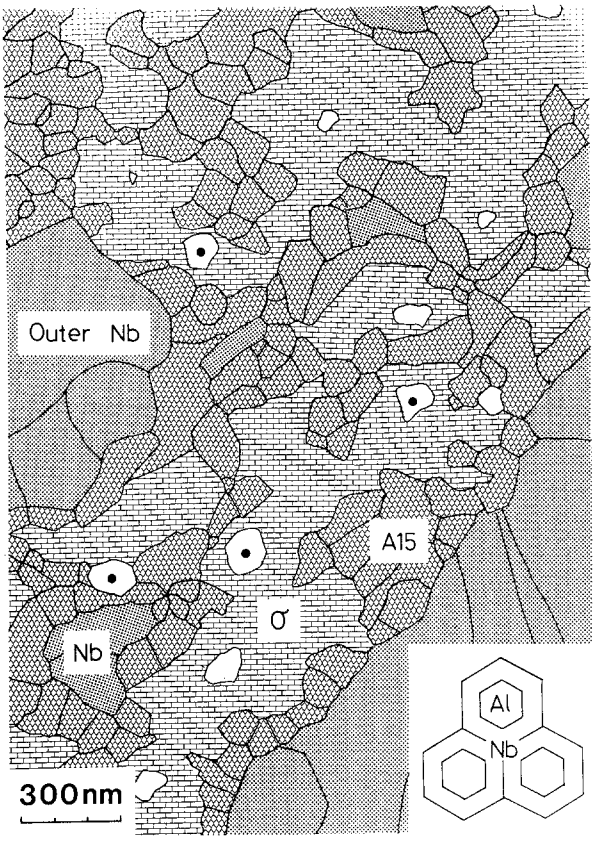

Figure 8 Schematic representation of cross-sectional phase distribution of sample 2 heat-treated at 1023 K for 86.4 ks. The hexagons indicate the initial Nb–Al composite size assuming closed packing in the 1st-level stack; (●) indicates perforation.

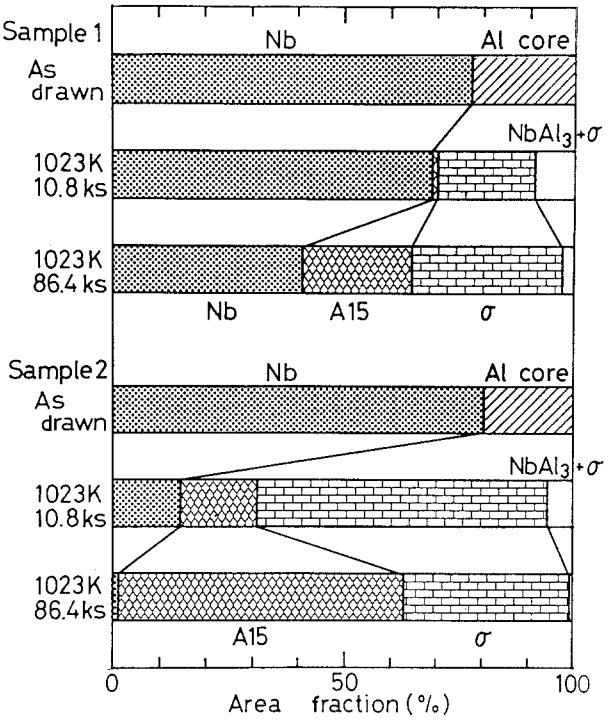

Figure 9 Area fraction of the reaction phases in a 1st-level stack.

The volume fraction of A15 increased with treatment time, consuming the Nb phase. The Al source during phase formation was the $NbAl_3$ phase. In sample 2 for 10.8 ks treatment, the volume fraction of σ phase was about 60% and A15 was about 20% of the 1st-level stack. After 86.4 ks treatment, the A15 phase grew by consuming Nb and σ phase. Since the diffusion length of sample 2 was shorter than that of sample 1, a large σ phase formed early and then σ phase dissolved and supplied A15 with Al during longer treatment.

The phase formation sequence almost agrees with the work of Barmak *et al.* [11], who suggested that σ phase formation proceeded concurrently with the formation of A15 in the multilayer of Nb–Al. On the other hand, preferential formation of the σ phase and voids in $NbAl_3$ were not reported in multilayer Nb–Al composites [11, 12]. The σ phase formation behaviour may be attributed to the initial configuration of the Nb–Al diffusion couple (mechanical alloying structure). The voids have been attributed to fast Al diffusion following the large areal reduction of the wire [17]. The addition of Cu to the Al core suppressed the Nb–Al interdiffusion reaction [18]. The effect of Cu on the phase formation could not be evaluated in this work. Further investigation is necessary to clarify the effect on the phase transformation.

3.4. Correlation between microstructure and superconducting properties

The superconducting properties of the wires (T_c, H_{c2} [7] and J_c [5]) are shown in Table IV. Fig. 9 and Table IV show the relationship between superconducting properties and the volume fraction of A15 in the 1st-level stack. The superconducting properties increased with A15 volume fraction. XRD study on the present multifilamentary wire showed that T_c was dominated by the development of A15 phase with a composition close to the stoichiometric [18]. The combination of a compositional approach to stoichiometry and an increase in the volume fraction brought about a remarkable increase in J_c.

One of the advantages of the Nb tube process over the other methods for Nb_3Al is that the fabricated conductor may be used for a.c. power applications

TABLE IV Superconducting properties of the samples

Sample	Heat treatment time at 1023 K (ks)	H_{c2}(4.2 K) [7] (T)	T_c [7] (K)	J_c(4.2 K, 8 T) [5][a] (10^9 A m^{-2})
Sample 1	10.8	9.6	12.2	
	86.4	17.3	14.2	0.12
Sample 2	10.8	17.25	14.0	0.35
	86.4	19.1	14.9	1.0

[a] "Sausaging" did not occur.

where a.c. losses must be extremely low. The continuous ultrafine filamentary structure is effective in reducing the a.c. loss. In order to really achieve these low a.c. losses, the filaments need, however, to be fully separated from each other for electromagnetic decoupling. Itoh *et al.* [8] revealed from magnetic susceptibility measurements that the effective diameter of superconducting filaments in a magnetic field was almost the same as the diameter of the 1st-level stack. The result indicated that there existed some electrocoupling layers between the Al cores.

The present TEM observations show that A15 filaments in the 1st-level stack coalesced with each other and formed a large aggregate. In order to separate the A15 filaments, the coalescence distance between Al cores was estimated from the average distance for region D in the heat-treated specimens. The distance was approximately 400 nm in sample 1 and 200 nm in sample 2. Approximately 800 nm may be required to separate the A15 filaments in sample 1 (Al core size: 320 nm) and 400 nm in sample 2 (Al core size: 120 nm). Based on this estimation, a recommended minimum Nb/Al atomic fraction in the starting composites will be 5.3 for sample 1 and 10 for sample 2. The higher Nb/Al ratio may be required in the smaller Al-core wire because the diffusion length Nb–Al may be in the range of 100 to 200 nm for the present heat treatments.

To prevent the coalescence of A15 filaments, a Cu or Ta sheath in the starting Nb–Al composite may be effective. The workability of the composite is important when fabricating a multifilamentary wire. Further investigation is required.

The distance between the Al cores became locally smaller than the average value, as seen in the micrographs. The inhomogeneous working process made the Al cores ribbon-shaped, rather than forming a uniform honeycomb structure. It is suggested from the present observations that another hydrostatic drawing process, as used for the commercial wire fabrication process, will be promising for improving a.c. losses.

4. Summary

TEM observations of transversal cross-sections of Nb–(Al– 2 at % Cu) multifilamentary wires were carried out. A sample preparation technique was developed for the transversal observation of multifilamentary wire by TEM. The following results were obtained.

1. Heavily deformed Al cores have a ribbon-like shape in the as-drawn specimen. A kind of mechanical alloying in the Al core was strongly suggested by the EDX analysis which revealed a ribbon-like morphology.

2. Intermetallic phases of $NbAl_3$, σ and A15 were found in the heat-treated specimen. Volume fractions of the phases were estimated from the transversal observation. The $NbAl_3$ and σ phases occupied a large part of the 1st-level stack in the early stage of the treatment. The volume fraction change produced by the heat treatment showed that σ formation was concurrent with the formation of the A15 phase, and that the A15 phase grew and coalesced by consuming Nb and σ phase.

3. The improvement of H_{c2} and J_c in a wire with a smaller Al core size is attributed to the larger volume fraction of A15. Coalescence of A15 phase in the 1st-level stack was directly observed. A larger A15 aggregate was formed in the smaller Al-core size wire. Interconnection between the microfilaments of A15 is attributed to inhomogeneous deformation of the single-core Nb–Al composite. A recommended Nb/Al ratio to separate the microfilaments is suggested.

Acknowledgement

The authors wish to thank Dr N. Kishimoto (NRIM) for his helpful advice.

References

1. T. ANDO, Y. TAKAHASHI, M. NISHI, Y. YAMADA, K. OHMATSU and M. NAGATA, *IEEE Trans. Magn.* **27** (1991) 1829.
2. K. INOUE, Y. IIJIMA and T. TAKEUCHI, *Appl. Phys. Lett.* **52** (1988) 1724.
3. S. CERESARA, M. V. RICCI, N. SACCHETTI and G. SACERDOTI, IEEE *Trans. Magn.* **MAG-11** (1975) 263.
4. R. AKIHAMA, R. J. MURPHY and S. FONER, *ibid.* **MAG-17** (1981) 274.
5. T. TAKEUCHI, Y. IIJIMA, M. KOSUGE, T. KURODA, M. YUYAMA and K. INOUE, *ibid.* **25** (1989) 2068.
6. T. KURODA, H. WADA, Y. IIJIMA and K. INOUE *J. Appl. Phys.* **65** (1989) 4445.
7. T. TAKEUCHI, M. KOSUGE, Y. IIJIMA, A. HASEGAWA, T. KIYOSHI and K. INOUE, *IEEE Trans Magn.* MAG-27 (1991) 2045.
8. K. ITOH, M. YUYAMA, T. KURODA, T. TAKEUCHI, M. KOSUGE and H. WADA, in "Proceedings of 11th International Conference on Magnet Technology", Tsukuba, Edited by T. Sekiguchi and S. Shimamoto (Elsevier, London, 1989) p. 962.
9. T. TAKEUCHI, Y. IIJIMA, M. KOSUGE, K. INOUE, K. WATANABE and K. NOTO, *Appl. Phys. Lett.* **53** (1988) 2444.
10. T. TAKEUCHI, M. KOSUGE, Y. IIJIMA, K. INOUE and K. WATANABE, *Adv. Cryogen, Engng* **36** (1990) 361.
11. K. BARMAK, K. R. COFFEY, D. A. RUDMAN and S. FONER, *J. Appl. Phys.* **67** (1990) 7313.
12. Y. IM and J.W. MORRIS Jr. *ibid.* **64** (1988) 3487.
13. W. E. KING, C. L. H. THINME and S. FONER: *IEEE Trans. Magn.* **MAG-21** (1985) 815.
14. Y. IM, P. E. JOHNSON, L. T. MCKNELLY, Jr and J.W. MORRIS Jr, *J. Less-Common Met.* **139** (1988) 87.
15. Y. WADAYAMA, T. SUZUKI, K. AIHARA, N. TADA, K. KAMATA, S. SAKAI and K. INOUE, *Appl. Phys. Lett.* **59** (1991) 473.
16. K. R. COFFEY, K. BARMAK, D. A. RUDMAN, C. L. H. THIEME and S. FONER, *IEEE Trans. Magn.* **MAG-25** (1989) 2093.
17. K. WATANABE, K. NOTO, H. MORITA, H. FUJIMORI and Y. MUTO, *ibid.* **MAG-25** (1989) 1984.
18. T. TAKEUCHI, M. KOSUGE, Y. IIJIMA, A. HASEGAWA, T. KIYOSHI, F. MATSUMOTO and K. INOUE, *J. Jpn Inst. Metals* **55** (1991) 472.

Received 2 September 1991
and accepted 30 March 1992